Deuteron gravitational form factors, generalized parton distributions, and charge density in the framework of the soft-wall AdS/QCD model

Shahin Mamedov a,b,c1, Minaya Allahverdiyeva b,c,d2, and Narmin Akbarova a,c3

- ^a Institute for Physical Problems, Baku State University, Z.Khalilov 23, Baku, AZ 1148, Azerbaijan
- ^b Institute of Physics, Ministry of Science and Education, H.Javid 33, Baku, AZ 1143, Azerbaijan
- ^c Center for Theoretical Physics, Khazar University, 41 Mehseti Str., Baku, AZ1096, Azerbaijan
 - ^d Western Caspian University, 31 Istiqlaliyyat Str., Baku, AZ1001, Azerbaijan

Abstract

We study the deuteron gravitational form factors (GFFs) and generalized parton distributions (GPDs) within the soft-wall AdS/QCD model, where deuteron is described by the bulk vector field with twist $\tau = 6$. For the finite-temperature studies, we apply the soft-wall model, which is thermalized by introducing a thermal dilaton field. GPDs and charge density are considered in impact parameter (IP) space and at zero and finite temperatures. We plot the temperature dependence of these quantities in IP space and observe a decreasing of their peaks on temperature increasing. The gravitational root means squared radius obtained here is close to the range given by experimental data for the mass radius and has low sensitivity to the temperature.

I. INTRODUCTION

Studying the internal structure of the deuteron has great importance for nuclear physics. The main theoretical tools in this study are the gravitational and electromagnetic form factors and the quantities related to them. GFFs supply information about the distribution of energy-momentum inside a hadron or nucleus and GPDs give information about parton distribution dependence on the fractional momentum of the parton. The GFFs are related to the GPDs. GFFs are determined as

¹ e-mail : sh.mamedov62@gmail.com

² e-mail : minaallahverdiyeva@ymail.com

³ e-mail : nerminh236@gmail.com

the form factors of energy-momentum tensor (EMT), which describes the interaction vertex in the graviton-deuteron elastic scattering. After the establishment of AdS/QCD models, which are based on the AdS/CFT correspondence principle [1–3], the different quantities of hadron phenomenology were successfully studied within these models [4–19]. Seminal works devoted to the study of the GFFs for the vector and spinor particles are [4–6], where the study was performed within the hard-wall model of AdS/QCD and the relation between GFFs and integrals over GPDs has also been shown. The hard-wall model GFFs for the vector field were extended to the deuteron case within the soft-wall model in Ref. [12]. Within the AdS/QCD, the electromagnetic form factors (EM FFs) of the deuteron were investigated in Refs. [7–9]. Several works were devoted to the deuteron study within the top-down approach of the holographic QCD as well ([51–54]).

The soft- and hard-wall models also have been applied in the study of the strong interaction coupling constants and form factors (FFs) of hadrons in the thermal medium [20–28]. In Refs. [21, 22] by making the dilaton field a thermal one, the soft-wall model has been extended to the non-zero temperature case and the explicit profile functions for the free boson and fermion fields interacted with the thermal dilaton field were found. Using this model the temperature dependence of the meson-nucleon coupling constants, nucleons axial-vector FFs, and vector meson GFFs and GPDs were studied at finite temperature case in Refs. [23–28]. In some physical situations the deuteron can turned out in the thermal medium, say in the Sun or heavy ion collisions. So, changing its properties depending on temperature has some significance for the in-medium studies. The thermalized soft-wall model opens an opportunity to study the deuteron GFFs at finite temperatures case too. Also, the temperature dependence of the deuteron's gravitational radius can be investigated using results for the thermal GFFs.

GPDs for the deuteron have been studied in Ref. [12] within the holographic soft-wall model, and contain results, which are similar to ones for the vector mesons. The deuteron GPDs were studied in the effective Lagrangian approach in Ref. [29] and employing GPDs the $G_C(Q^2)$, $G_M(Q^2)$, and $G_Q(Q^2)$ form factors were obtained. The GPDs appear in processes of deeply virtual Compton scattering (DVCS) or vector meson productions [30–33] and they give the ordinary parton distributions in the forward limit. GPDs for deuteron were introduced in Ref. [34] and studied theoretically in Refs. [35–43]. In Ref. [4] the GPDs were related to holographic GFFs for the spin 1 and 1/2 particles. In the holographic framework the deuteron's GPDs have been obtained from the EM FFs in Ref. [12]. Alternatively, the deuteron GPDs can be obtained from GFFs within the AdS/QCD framework and studied. So, it is interesting to derive the GPDs from the GFFs and compare them with the ones obtained from the EM FFs. The GPDs for ρ mesons were

obtained from the GFFs within the soft-wall model at zero and finite temperature cases in Ref. [26] AdS/QCD. The soft-wall model opens wide opportunities for the study of GPDs at zero and non-zero temperatures [26].

Charge density for the transversally polarized deuteron [12] was obtained from EM FFs within the soft-wall model. For the unpolarized ρ mesons this density was derived from the GFFs within both hard- and soft-wall models [6]. In Ref. [12] a holographic study of deuteron GFFs was carried out as well. Following these works the charge density for the unpolarized deuteron can be obtained from the GFFs within the holographic models. Finite-temperature soft-wall model opens an opportunity to study the temperature dependence of the deuteron's charge density as well.

The impact parameter (IP) shows the separation of the struck quark from the center of momentum and the soft-wall study of the deuteron's GPDs and charge density can be extended to the IP space. Within the soft-wall AdS/QCD model the deuteron's charge density was plotted in two-dimensional graphs in Ref. [12]. The transverse charge density transversely polarized deuteron within the soft-wall model was studied in Ref. [50] It is possible to extend this plot to three dimensions and finite-temperature cases as well.

The paper is organized in the following: In section II, we present the basic elements of the soft-wall model and study the deuteron GFFs and gravitational radius at zero and finite temperature cases. In section III, we study deuteron GPDs obtained from the GFFs and consider their temperature dependence. In section IV, we investigate deuteron GPDs in IP space at zero and finite temperatures. In section V, we calculate the deuteron charge density at zero and finite temperature. We summarize our results for the deuteron GFFs, GPDs, and charge density in the last section.

II. DEUTERON GFFS AT ZERO AND FINITE TEMPERATURES

The background geometry for the model is the 5-dimensional (5D) AdS space with the radius R = 1, which is given by the following line element in Poincare coordinates:

$$ds^{2} = g_{MN}dx^{M}dx^{N} = \frac{1}{z^{2}} \left(-dz^{2} + (\eta_{\mu\nu} + h_{\mu\nu})dx^{\mu}dx^{\nu} \right), \quad \mu, \nu = 0, 1, 2, 3; \quad M, N = 0, 1, 2, 3, 5.$$
(2.1)

Here $\eta_{\mu\nu}=diag(1,-1,-1,-1)$ is the 4-dimensional Minkowski metric and z is the holographic coordinate varying in the range $\epsilon \leq z < \infty$. $h_{\mu\nu}$ is the perturbation of the metric and $h_{5N}=0$.

Finiteness of the 5D action is provided by introducing an exponential dilaton field $e^{-\Phi(z)}$ with

 $\Phi(z) = k^2 z^2$, which suppresses expressions under the integral over z at infinity. This field also provides the dual QCD theory's confinement and chiral symmetry-breaking properties. For the k parameter we take value $k = 190 \text{ MeV} = 0.9 \text{ fm}^{-1}$ which applied in Refs. [10, 12] and fixed by fitting the electromagnetic form factors of the deuteron with experimental data.

Action for the model of deuteron interacting with the graviton will be written as:

$$S = \int_{0}^{\infty} d^{4}x dz e^{-\Phi(z)} \sqrt{g} \left[L_{d}(x, z) + L_{g}(x, z) \right], \tag{2.2}$$

where $L_d(x,z) = -D^M d_N^{\dagger} D_M d^N + d_M^{\dagger} \left(\mu^2 + U(z) \right) d^M$ is a deuteron lagrangian and

$$\mu^2 = (\Delta - 1)(\Delta - 3) = (L + 5)(L + 3).$$

Here $\Delta = \tau + L$ is the conformal dimension of the bulk vector field $d^N(x,z)$ describing the deuteron in the boundary theory, $L = max|L_z|$ is the maximal value of the z component orbital angular momentum of the quark field. $L_g(x,z) = R+12$ in the Eq (2.2) is the lagrangian for gravity sector, R is the Ricci scalar, $g = |\det g_{MN}|$. The potential U(z) for the deuteron was found in Ref. [8] and has the explicit form $U(z) = \phi(z)U_0$, where the value $U_0 = 87.4494$ was fixed by the mass of the deuteron.

A. GFFs for the deuteron at zero temperature

Following Refs. [7–9] we describe deuteron by the twist $\tau = 6$ vector field d_N with $d_5 = 0$. Similarly to the spin-1 particles the matrix elements of the light-front energy-momentum stress tensor operator $T^{++}(0)$ between the deuteron's initial and final states are expressed by the gravitational form factor $\mathcal{T}_{\lambda_2\lambda_1}^+(Q^2)[6, 12]$:

$$\left\langle p^{+}, \frac{\mathbf{q}_{\perp}}{2}, \lambda_{2} \middle| T^{++}(0) \middle| p^{+}, -\frac{\mathbf{q}_{\perp}}{2}, \lambda_{1} \right\rangle$$

$$= 2(p^{+})^{2} e^{i(\lambda_{1} - \lambda_{2})\phi_{q}} \mathcal{T}_{\lambda_{2}\lambda_{1}}^{+}(Q^{2}). \tag{2.3}$$

Fourier transform of the $\mathcal{T}^+_{\lambda_2\lambda_1}(Q^2)$ form factor gives the p^+ gravitomagnetic momentum density in the transverse plane $(p^+ = \frac{p^0 + p^3}{\sqrt{2}})$. Here λ_1 and λ_2 are the light-front helicities of the deuteron's initial and final states, $\mathbf{q}_{\perp} = Q(\cos\phi_q\hat{e}_x + \sin\phi_q\hat{e}_y)$. We shall use the unpolarized case, where $\left|\mathbf{q}_{\perp}\right| = Q$ for the $\lambda_{1,2} = 1$ and $\lambda_{1,2} = 0$ states.

There are two independent helicity conserving FFs \mathcal{T}_{00}^+ and $\mathcal{T}_{11}^+(Q^2)$ are equal to the Z_1 and Z_2

functions respectively, which and have the forms below [6, 12]:

$$\mathcal{T}_{00}^{+}(Q^{2}) = Z_{1}(Q) = \int \frac{dz}{z} e^{-k^{2}z^{2}} H(Q, z) \partial_{z} \psi_{n}(z) \partial_{z} \psi_{n}(z) ,$$

$$\mathcal{T}_{11}^{+}(Q^{2}) = Z_{2}(Q) = \int \frac{dz}{z} e^{-k^{2}z^{2}} H(Q, z) \psi_{n}(z) \psi_{n}(z) .$$
(2.4)

Here H(Q, z) is the bulk-to-boundary propagator for the graviton and $\psi_n(z)$ is the *n*-th mode's profile function in the deuteron d_N wave function's Kaluza-Klein decomposition. An explicit expression for this propagator was obtained in Ref. [4]:

$$H(Q,z) = \Gamma(a+2)U(a,-1;2k^2z^2) = a(a+1)\int_0^1 dx \, x^{a-1}(1-x) \exp\left(-\frac{2k^2z^2x}{1-x}\right). \tag{2.5}$$

In Ref. [26] it was reduced to the following form:

$$H(Q,z) = 4 \int_0^1 dx k^4 z^4 \frac{x^{a+1}}{(1-x)^3} \exp\left(-\frac{2k^2 z^2 x}{1-x}\right),$$
 (2.6)

where $a = \frac{Q^2}{8k^2}$. The $\psi_n(z)$ profiles are found by solving the equation of motion for the deuteron field and have expressed in terms of generalized Laguerre polynomials $L_n^{(\alpha)}$ in Refs. [7, 8]:

$$\psi_n(z) = \sqrt{\frac{2\Gamma(n+1)}{\Gamma(n+L+5)}} k^{L+5} z^{L+9/2} L_n^{L+4} (k^2 z^2).$$
 (2.7)

We shall consider the ground state of the deuteron, i.e. n = 0, L = 0, and $L_0^4 = 1$. Using these expressions for $\psi(z)$ and H(Q, z) the integral over z and x in the $Z_{1,2}(Q)$ form factors can be taken and their analytic expressions are found in the following:

$$Z_{1}(Q) = \left\{ 256k^{4}(16k^{2} + Q^{2})(24k^{2} + Q^{2})(32k^{2} + Q^{2})(40k^{2} + Q^{2}) \right\}^{-1} \left\{ (40k^{2} + Q^{2})(3342336k^{12} + 81920k^{10}Q^{2} + 159104k^{8}Q^{4} + 15600k^{6}Q^{6} + 1284k^{4}Q^{8} + 40k^{2}Q^{10} + Q^{12}) + 2Q^{2}(8k^{2} + Q^{2})(18432k^{8} + 3584k^{6}Q^{2} + 512k^{4}Q^{4} + 16k^{2}Q^{6} + Q^{8})_{2}F_{1}(1, 2 + a, 7 + a, -1) \right\},$$

$$(2.8)$$

$$Z_{2}(Q) = \left\{ 4k^{2}(16k^{2} + Q^{2})(24k^{2} + Q^{2})(32k^{2} + Q^{2})(40k^{2} + Q^{2})(48k^{2} + Q^{2}) \right\}^{-1} \left\{ (48k^{2} + Q^{2})(1966080k^{10} - 177152k^{8}Q^{2} + 8576k^{6}Q^{4} - 672k^{4}Q^{6} + 4k^{2}Q^{8} - Q^{10}) + 2Q^{2}(8k^{2} + Q^{2})(18432k^{8} + 3584k^{6}Q^{2} + 512k^{4}Q^{4} + 16k^{2}Q^{6} + Q^{8})_{2}F_{1}(1, 2 + a, 7 + a, -1) \right\}.$$

$$(2.9)$$

The gravitational root mean square (RMS) radius is defined by taking the derivative from the gravitational form factor $Z_2(Q^2)$ [4]:

$$\langle r^2 \rangle_{\text{grav}} = -6 \left. \frac{\partial Z_2(Q)}{\partial Q^2} \right|_{Q^2 = 0}.$$
 (2.10)

Value of the gravitational RMS radius is found from Z_2 by use of this definition:

$$\langle r^2 \rangle_{\text{grav}} = 1.605 \text{ fm}^2.$$
 (2.11)

For the radius, we find $r_{\rm grav} = \sqrt{\langle r^2 \rangle_{\rm grav}} = 1.26$ fm. In CLAS experiment of electroproduction of ϕ meson in the process $\gamma + d \to d + \phi$ in two different ranges of photon energies $E_{\gamma} = 1.6 - 2.6$ GeV and $E_{\gamma} = 2.6 - 3.6$ GeV it were found values for the deuteron mass radius $r_{exp} = 1.94 \pm 0.45$ fm and 1.78 ± 0.38 fm respectively, [46]. $r_{\rm grav}$ found here close to the lowest experimental value for the mass radius r_{exp} .

B. Deuteron GFFs at finite temperature

In Refs. [21, 22] the soft-wall model was extended to the finite temperature case by introducing the warping factor $\exp[-\phi(z,T)]$, which depends on temperature. The temperature dependence in such a model was achieved by considering the dilaton constant k as the temperature-dependent one, i.e. the dilaton field in this model is $\phi(z,T) = K^2(T)z^2$. The action for the soft-wall model is written in terms of such a dilaton field:

$$S = \int_{0}^{\infty} d^4x dz \sqrt{g} e^{-\phi(z,T)} \mathcal{L}(x,z,T). \qquad (2.12)$$

Here $\mathcal{L}(x, z, T)$ is the temperature-dependent Lagrangian, and $g = |\det g_{MN}|$ is the determinant of the g_{MN} metric of the AdS-Schwarzschild space with line element:

$$ds^{2} = e^{2A(z)} \left[-f(z)dt^{2} - (d\vec{x})^{2} - \frac{dz^{2}}{f(z)} \right], \quad f(z) = 1 - \frac{z^{4}}{z_{H}^{4}}.$$
 (2.13)

Here $A(z) = -\log z$, z_H is the position of the event horizon, which defines the temperature $T = \frac{1}{\pi z_H}$. In this model it is suitable to apply the Regge-Wheeler tortoise coordinate r related to z and the thermal factor $f_T(r)$ in terms of the r coordinate has the same form as in z coordinate, Ref. [21], i.e.

$$f_T(r) = 1 - \frac{r^4}{z_H^4}. (2.14)$$

In terms of the r coordinate the metric of the AdS-Schwarzschild space-time is written with $A(r) = -\log r$ as below:

$$ds^{2} = e^{2A(r)} f_{T}^{\frac{3}{5}}(r) \left[dt^{2} - \frac{(d\vec{x})^{2}}{f_{T}(r)} - dr^{2} \right]$$
(2.15)

and the dilaton field $\phi(r,T)$ becomes:

$$\phi(r,T) = K^{2}(T)r^{2}, \quad K^{2}(T) = k^{2}[1 + \rho(T)], \tag{2.16}$$

$$\rho(T) = \delta_{T1} \frac{T^2}{12F^2} + \delta_{T2} \left(\frac{T^2}{12F^2}\right)^2, \tag{2.17}$$

where $\delta_{T1} = -\frac{N_f^2 - 1}{N_f}$ and $\delta_{T2} = -\frac{N_f^2 - 1}{2N_f^2}$ are the constants, and $F = k\frac{\sqrt{3}}{8}$ is the pseudoscalar meson decay constant at zero temperature and in the chiral limit, and N_f is the number of quark flavors [21, 22].

In the case of zero temperature, the deuteron profile function was studied within the soft-wall model in [7, 8]. Following the Refs. [21, 22], where the meson and baryon profile functions were derived at finite temperature, we derive the deuteron profile derivation at finite temperature case within the soft-wall model. Similarly to the T=0 case, we write action for the bulk vector field d with the twist $\tau=6$ and spin J=1, which describes the deuteron field at the UV boundary of the AdS-Schwarzchild space-time:

$$S = \int_{0}^{\infty} d^{4}x dr e^{-\phi(r,T)} \sqrt{g} \left[-(D^{M} d_{N}(x,r,T))^{+} D_{M} d^{N}(x,r,T) + \left(\mu^{2}(r,T) + V(r,T) \right) d_{M}^{+}(x,r,T) d^{M}(x,r,T) \right].$$
(2.18)

The covariant derivative $D^M = \partial^M - ieV^M(r,T)$ in our free deuteron field case is just ∂^M . The thermal dilaton potential for the d^M field has a form:

$$V(r,T) = \frac{4}{f_T^{3/5}(r)} K_T^2 r^2, \tag{2.19}$$

and the temperature-dependent bulk mass $\mu^2(r,T)$ is related to the zero-temperature mass μ^2 :

$$\mu^{2}(r,T) = \frac{\mu^{2}}{f_{T}^{3/5}(r)}.$$
(2.20)

We use the axial gauge condition for the d field $d^z(x,r,T)=0$. Notice that $\partial_\alpha \partial^\beta d^\nu(x,r,T) \eta^{\alpha\beta}=-M^2 d^\nu(x,r,T)$, where M is the mass of the deuteron. Kaluza-Klein (KK) decomposition for the d^ν field is written as

$$d^{\nu}(x, r, T) = e^{(\phi(r, T) - A(r))/2} \sum_{n} d_{n}^{\nu}(x) \psi_{n}(r, T)$$
(2.21)

and the $d_{n}^{\nu}\left(x\right)$ tower of KK components dual to the deuteron states with the radial quantum number n.

The EOM for the $\psi_n(r,T)$ mode will be obtained from the action (2.18). Explicit equation for the deuteron modes can be written from the general equation for mesons with the spin J by taking J=1 in it [7]. This equation is the Schrödinger-type equation:

$$\left[-\frac{d^2}{dr^2} + k^4 r^2 \left(1 + 2\rho(T) \right) + \frac{4m^2 - 1}{4r^2} - 4k^2 \left(1 + \rho(T) \right) \left(n + \frac{m+1}{2} \right) \right] \psi_{nm} \left(r, T \right) = 0.$$
 (2.22)

Here m = 4 + L. Solution to this equation - profile function $\psi_{nm}(r,T)$ for the *n*-th mode of the deuteron has a form:

$$\psi_{nm}(r,T) = \sqrt{\frac{2\Gamma(n+1)}{\Gamma(n+m+1)}} K_T^{m+1} r^{m+1/2} e^{-K_T^2 r^2/2} L_n^m \left(K_T^2 r^2/2 \right).$$

For the ground state with n = 0 and L = 0, we have the finite-temperature profile function below:

$$\psi(r,T) = \sqrt{\frac{2}{4!}} K_T^5 r^{9/2} e^{-K_T^2 r^2/2}.$$
 (2.23)

This solution coincides with one obtained in [12] for the zero-temperature case by making replacements $K_T \to k$ and $r \to z$. Analogously to zero-temperature case, the form-factors $Z_1(Q^2, T)$ and $Z_2(Q^2, T)$ are written in terms of the deuteron profile function $\psi(r, T)$ and graviton bulk-to-boundary propagator H(Q, T, r):

$$\mathcal{T}_{00}^{+}(Q^{2},T) = Z_{1}(Q^{2},T) = \int dr H(Q,T,r) \partial_{r} \psi(r,T) \partial_{r} \psi(r,T) ,$$

$$\mathcal{T}_{11}^{+}(Q^{2},T) = Z_{2}(Q^{2},T) = \int dr H(Q,T,r) \psi(r,T) \psi(r,T) . \qquad (2.24)$$

The finite-temperature graviton bulk-to-boundary propagator H(Q, T, r) was obtained by solving the EOM at finite temperature, which is obtained from the EOM at zero temperature by the replacements $k \to K_T$ and $z \to r$. So, the solution H(Q, T, r) differs from the H(Q, z) by this replacement ([26]):

$$H(Q,T,r) = \Gamma(a_T + 2)U(a_T, -1; 2K_T^2r^2) =$$

$$= a_T(a_T + 1) \int_0^1 dx \, x^{a_T - 1} (1 - x) \exp\left(\frac{-2K_T^2r^2x}{1 - x}\right) =$$

$$= 4 \int_0^1 dx K_T^4 r^4 \frac{x^{a_T + 1}}{(1 - x)^3} \exp\left(\frac{-2K_T^2r^2x}{1 - x}\right), \tag{2.25}$$

where $a_T = \frac{Q^2}{8K_T^2}$. Having plotted the Q^2 and T dependencies of the $Z_{1,2}(Q^2,T)$ form factors in Fig. 1 and Fig. 2 we visualize the temperature impact on the energy-momentum distribution of partons inside the deuteron. Plots for the GFFs in Fig.1 show very weak temperature dependencies of these form factors. This means, that temperature weakly affects the distribution of energy and momentum inside the deuteron.

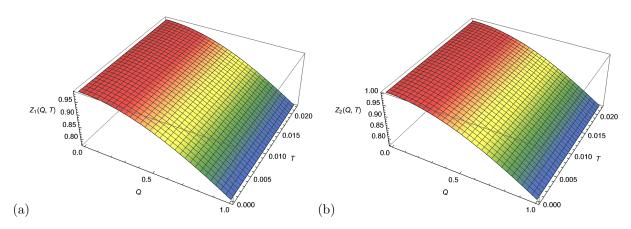


FIG. 1: Plots of (a) $Z_1(Q^2, T)$ form factor and (b) $Z_2(Q^2, T)$ form factor at finite temperature for the deuteron in fm units.

Using the finite-temperature expression for $Z_2(Q^2,T)$ we can find the deuteron gravitational radius at finite temperature by taking the derivative from this gravitational form factor:

$$\left\langle r^2(T) \right\rangle_{\text{grav}} = -6 \left. \frac{\partial Z_2(Q, T)}{\partial Q^2} \right|_{Q^2 = 0}.$$
 (2.26)

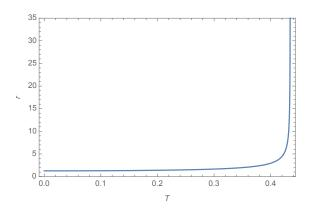


FIG. 2: Plot of gravitational RMS radius for the deuteron.

As is seen from Fig. 2 the RMS radius plot increases on increasing medium temperature starting from $r_{\rm grav}=1.26$ fm at T=0 value. Starting from the temperature $T\approx 0.21$ fm⁻¹ the radius grows quickly and becomes infinite at the temperature $T\sim 0.42$ fm⁻¹. Such graph behavior can be related to the change of structure in the deuteron. As is known [48] the binding energy for the deuteron is $\sim T=2.22$ MeV $\simeq 0.11$ fm⁻¹ and it has no excited states. At the temperature equal to $T\simeq 0.11$ fm⁻¹ temperature, the deuteron splits into the proton and neutron and does not behave as a single particle. So, only T<0.11 fm⁻¹ part of this graph describes the deuteron.

III. DEUTERON GPDS

GPDs describe the distributions of partons inside the hadron and are the functions of the longitudinal momentum fraction x of the active quark or gluon, skewness ξ and Q^2 . Here we shall not study the skewness dependence of the GPDs. Within the hard-wall model of AdS/QCD GPDs for the vector field were written in Ref. [4] and were related to holographic GFFs. (The study of deuteron's GPDs within the soft-wall model was done in Ref. [12] with the EM FFs study.) We aim to obtain the deuteron GPDs from GFFs using the relation between them, which was applied in Ref. [4] for the vector field. The GFFs study for the vector field was extended to the soft-wall model and the non-zero temperature case in Ref. [26]. Similar research can be done for the deuteron as well, taking the twist of the vector field $\tau = 6$. For the n-th deuteron state d_n the GFFs are defined by the following matrix element of $\hat{T}^{\mu\nu}$ - the transverse-traceless part of energy-momentum stress tensor $T^{\mu\nu}$:

$$\left\langle d_{n}^{a}(p_{2},\lambda_{2}) \middle| \hat{T}^{\mu\nu}(q) \middle| d_{n}^{b}(p_{1},\lambda_{1}) \right\rangle = \\
(2\pi)^{4} \delta^{(4)}(q+p_{1}-p_{2}) \delta^{ab} \varepsilon_{2\alpha}^{*} \varepsilon_{1\beta} \\
\times \left[-A(q^{2}) \left(4q^{[\alpha} \eta^{\beta](\mu} p^{\nu)} + 2\eta^{\alpha\beta} p^{\mu} p^{\nu} \right) \right. \\
\left. - \frac{1}{2} \hat{C}(q^{2}) \eta^{\alpha\beta} \left(q^{2} \eta^{\mu\nu} - q^{\mu} q^{\nu} \right) \right. \\
+ D(q^{2}) \left(q^{2} \eta^{\alpha(\mu} \eta^{\nu)\beta} - 2q^{(\mu} \eta^{\nu)(\alpha} q^{\beta)} + \eta^{\mu\nu} q^{\alpha} q^{\beta} \right) \\
- \hat{F}(q^{2}) \frac{q^{\alpha} q^{\beta}}{m_{n}^{2}} \left(q^{2} \eta^{\mu\nu} - q^{\mu} q^{\nu} \right) \right], \tag{3.1}$$

where m_n is the mass of the d_n state. The FFs A, \hat{C}, D, \hat{F} are composed from the invariant functions Z_1 and Z_2 :

$$A(q^{2}) = Z_{2},$$

$$\hat{C}(q^{2}) = \frac{1}{q^{2}} \left(\frac{4}{3} Z_{1} + \left(q^{2} - \frac{8m_{n}^{2}}{3} \right) Z_{2} \right),$$

$$D(q^{2}) = \frac{2}{q^{2}} Z_{1} + \left(1 - \frac{2m_{n}^{2}}{q^{2}} \right) Z_{2},$$

$$\hat{F}(q^{2}) = \frac{4m_{\rho}^{2}}{3q^{4}} \left(Z_{1} - m_{n}^{2} Z_{2} \right).$$
(3.2)

Generally, there are five GPDs for the spin-1 particles, which are expressed with the matrix

element of the QCD non-local and non-diagonal operators on the light-front [4, 12, 44]:

$$\int \frac{p^{+}dy^{-}}{2\pi} e^{ixp^{+}y^{-}} \times
\langle p_{2}, \lambda_{2} | \bar{q}(-\frac{y}{2})\gamma^{+}q(\frac{y}{2}) | p_{1}, \lambda_{1} \rangle_{y^{+}=0, y_{\perp}=0}
= -2(\varepsilon_{2}^{*} \cdot \varepsilon_{1})p^{+}H_{1}(x, \xi, t) - (\varepsilon_{1}^{+} \varepsilon_{2}^{*} \cdot q - \varepsilon_{2}^{+*} \varepsilon_{1} \cdot q) H_{2}(x, \xi, t)
+ q \cdot \varepsilon_{1} q \cdot \varepsilon_{2}^{*} \frac{p^{+}}{m_{n}^{2}} H_{3}(x, \xi, t) - (\varepsilon_{1}^{+} \varepsilon_{2}^{*} \cdot q + \varepsilon_{2}^{+*} \varepsilon_{1} \cdot q) H_{4}(x, \xi, t)
+ \left(\frac{m_{n}^{2}}{(p^{+})^{2}} \varepsilon_{1}^{+} \varepsilon_{2}^{+*} + \frac{1}{3} (\varepsilon_{2}^{*} \cdot \varepsilon_{1})\right) 2p^{+} H_{5}(x, \xi, t) ,$$
(3.3)

where x is a momentum fraction $x = \frac{k^+}{p^+}$ varying in the interval $-1 \le x \le 1$, k^+ is the parton's (quark's) light-cone momentum, ξ is a skewness $\xi = -\frac{q^+}{2p^+}$, and valence quark GPDs H_i^v are defined by H_i as $H_i^v(x,0,t) = H_i(x,0,t) + H_i(-x,0,t)$.

The first moments of deuteron's H_i GPDs for the valence quark are related to the linear combinations of the A, B, C, D, E form factors in (3.1) in the following [4, 44]:

$$\int_{-1}^{1} x dx \, H_{1}(x,\xi,t) = A(t) - \xi^{2}C(t) + \frac{t}{6m_{\rho}^{2}}D(t),$$

$$\int_{-1}^{1} x dx \, H_{2}(x,\xi,t) = 2\left(A(t) + B(t)\right),$$

$$\int_{-1}^{1} x dx \, H_{3}(x,\xi,t) = E(t) + 4\xi^{2}F(t),$$

$$\int_{-1}^{1} x dx \, H_{4}(x,\xi,t) = -2\xi D(t),$$

$$\int_{-1}^{1} x dx \, H_{5}(x,\xi,t) = +\frac{t}{2m_{\rho}^{2}}D(t).$$
(3.4)

Using the explicit expression for $\psi(z)$ in Eq. (2.4) and H(Q,z) in Eq. (2.6) the integral expression for the Z_1, Z_2 GFFs can be found:

$$Z_{1}(Q) = \int_{0}^{1} dx \int_{0}^{\infty} dz k^{14} z^{11} \frac{8x^{(a+1)}}{(1-x)^{3}} e^{\frac{-k^{2}z^{2}(1+x)}{1-x}},$$

$$Z_{2}(Q) = \int_{0}^{1} dx \int_{0}^{\infty} dz k^{14} z^{13} \frac{x^{(a+1)}}{3(1-x)^{3}} e^{\frac{-k^{2}z^{2}(1+x)}{1-x}}.$$
(3.5)

Taking into account Eq. (3.5) in Eq. (3.2) and the obtained result in Eq. (3.4) we obtain an expression for the deuteron GPDs for $\xi = 0$:

$$H_1^v(x,0,t) = -\frac{5(1-x)^3(4(4m^2+t)(1-x)+27k^2(1+x))}{m^2(1+x)^7}x^{-a},$$

$$H_2^v(x,0,t) = -\frac{240(x-1)^4}{(1+x)^7}x^{-a},$$

$$H_5^v(x,0,t) = -\frac{15(x-1)^3(4(2m^2-t)(x-1)+27k^2(1+x))}{m^2(1+x)^7}x^{-a},$$
(3.6)

where $t = -Q^2$.

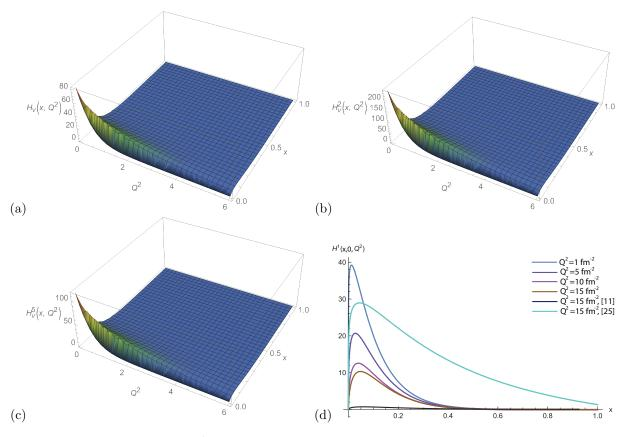


FIG. 3: Plot of $H^i_v(x,0,t)$ is generalized parton distributions for deuteron.

It is seen from Fig. 3 the H_v^i GPDs have peak near the $(x = 0, Q^2 = 0)$ point. Such a peak and shape have the GPDs obtained from the EM FFs of the deuteron in Ref. [12].

The deuteron GPDs H_i at zero temperature can easily be extended to the finite temperature case by applying the temperature-dependent propagator H(Q,T,r). Integral representation for H(Q,T,r) is obtained by replacing the dilaton constant κ by K_T and the z coordinate by the r tortoise one in the zero-temperature expression (2.6):

$$H(Q,T,r) = 4 \int_0^1 dx K_T^4 r^4 \frac{x^{a_T+1}}{(1-x)^3} e^{\frac{-2K_T^2 r^2 x}{1-x}}.$$
 (3.7)

So, finite-temperature version of GPDs (3.5) will be written as:

$$H_1^v(x,0,t,T) = -\frac{5(1-x)^3(4(4m^2+t)(1-x)+27K_Tr(1+x))}{m^2(1+x)^7}x^{-a_T}.$$
 (3.8)

The GFFs in terms of H(Q, T, r) read

$$Z_{1}(Q,T) = \int_{0}^{1} dx \int_{0}^{\infty} dr K_{T}^{14} r^{11} \frac{8x^{(a_{T}+1)}}{(1-x)^{3}} e^{\frac{-K_{T}^{2} r^{2}(1+x)}{1-x}},$$

$$Z_{2}(Q,T) = \int_{0}^{1} dx \int_{0}^{\infty} dr K_{T}^{14} r^{13} \frac{x^{(a_{T}+1)}}{3(1-x)^{3}} e^{\frac{-K_{T}^{2} r^{2}(1+x)}{1-x}}.$$
(3.9)

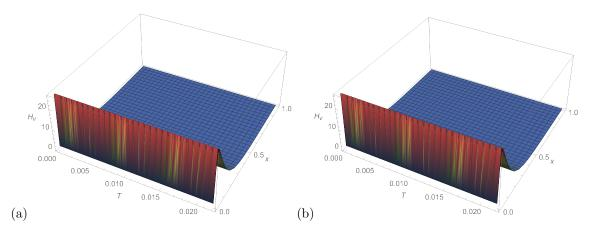


FIG. 4: Plot of $H_v^1(x,0,t,T)$ is generalized parton distributions at finite temperature. Accordingly, (a) is $Q^2 = 1$ fm⁻² and (b) is $Q^2 = 3$ fm⁻².

As is seen from Fig.4, both GPDs have a maximum at $x \approx 0.2$ and temperature weakly affects these maxima. Such a maximum can be met in Ref. [47] (Fig. 1), where GPDs were studied for the u and d quarks at zero temperature within the hard-wall model. Also, a holographic study of the deuteron GPDs obtained from the EM FF within the soft-wall model indicates the presence of deuteron GPDs maxima near $x \approx 0.2$ ([12], Fig. 8 (b)). In addition, this maximum is present in vector meson GPDs as well ([26]). This peak can be seen in zero-temperature plots in Fig. 3 (d) as well.

IV. DEUTERON GPDS IN IP SPACE

The IP-dependent parton distribution functions (PDFs) for a quark of momentum fraction x located in the transverse position \mathbf{b}_{\perp} in the impact parameter space gives a picture of the distribution of quark charge densities inside the deuteron through $H_i(x, \mathbf{b}_{\perp})$. Utilizing the GPDs in impact parameter space, one can calculate the distributions of partons in the transverse plane, which is significant for the study of deuteron's structure. To localize the deuteron in the transverse direction, one needs to put the transverse center of momentum \mathbf{R}_{\perp} at the origin, and such a state in the transverse center of momentum is defined as [45]:

$$|p^+, \mathbf{R}_{\perp} = \mathbf{0}_{\perp}, \lambda\rangle \equiv \mathcal{N} \int \frac{d^2 \mathbf{p}_{\perp}}{(2\pi)^2} |p^+, \mathbf{p}_{\perp}, \lambda\rangle.$$
 (4.1)

The normalization constant \mathcal{N} is found from the normalization $|\mathcal{N}|^2 \int \frac{d^2 \mathbf{p}_{\perp}}{(2\pi)^2} = 1$. $|p^+, \mathbf{p}_{\perp}, \lambda\rangle$ are light-cone helicity eigenstates of the deuteron. Thus, one can define deuteron GPDs in IP space

 $H_i(x, \mathbf{b}_{\perp})$:

$$H(x, \mathbf{b}_{\perp}) \equiv \left\langle p^{+}, \mathbf{R}_{\perp} = \mathbf{0}_{\perp}, \lambda \right| \int \frac{dy^{-}}{4\pi} \bar{q} \left(-\frac{y^{-}}{2}, \mathbf{b}_{\perp} \right) \gamma^{+} q \left(\frac{y^{-}}{2}, \mathbf{b}_{\perp} \right) \left| p^{+}, \mathbf{R}_{\perp} = \mathbf{0}_{\perp}, \lambda \right\rangle e^{ixp^{+}y^{-}}$$

$$= |\mathcal{N}|^{2} \int \frac{d^{2}\mathbf{p}_{\perp}}{(2\pi)^{2}} \int \frac{d^{2}\mathbf{p}_{\perp}'}{(2\pi)^{2}} \left\langle p^{+}, \mathbf{p}_{\perp}', \lambda \right| \int \frac{dy^{-}}{4\pi} \bar{q} \left(-\frac{y^{-}}{2}, \mathbf{0}_{\perp} \right) \gamma^{+} q \left(\frac{y^{-}}{2}, \mathbf{0}_{\perp} \right) \left| p^{+}, \mathbf{b}_{\perp}, \lambda \right\rangle e^{i\mathbf{b}_{\perp}(\mathbf{p}_{\perp} - \mathbf{p}_{\perp}')} e^{ixp^{+}y^{-}}.$$

$$(4.2)$$

To illustrate the physics of GPDs $H_i^v(x, 0, q)$, we take the definition of IP-dependent parton distribution functions (PDFs):

$$H(x, \mathbf{b}_{\perp}) = |\mathcal{N}|^2 \int \frac{d^2 \mathbf{p}_{\perp}}{(2\pi)^2} \int \frac{d^2 \mathbf{p}_{\perp}'}{(2\pi)^2} H^{\nu}(x, 0, \mathbf{q}_{\perp}^2) e^{i\mathbf{b}_{\perp}(\mathbf{p}_{\perp} - \mathbf{p}_{\perp}')}$$
$$= \int \frac{d^2 \mathbf{q}_{\perp}}{(2\pi)^2} H^{\nu}(x, 0, \mathbf{q}_{\perp}^2) e^{-i\mathbf{b}_{\perp}\mathbf{q}_{\perp}}, \tag{4.3}$$

where \mathbf{b}_{\perp} is the IP and $|\mathbf{b}_{\perp}| = b$ is a measure of the transverse distance between the struck parton and the transverse center of momentum of the hadron, $\mathbf{q}_{\perp} = \mathbf{p}'_{\perp} - \mathbf{p}_{\perp}$. As is shown in Ref. [45], GPDs in the momentum space are related to the IP-dependent parton distributions via the Fourier transform:

$$H_i(x, \mathbf{b}_\perp) = \int_0^\infty \frac{d^2 \mathbf{q}_\perp}{(2\pi)^2} H_i^v(x, 0, \mathbf{q}_\perp^2) e^{-i\mathbf{b}_\perp \mathbf{q}_\perp}.$$
 (4.4)

After integrating over the angle between the \mathbf{b}_{\perp} and \mathbf{q}_{\perp} vectors $H_i(x, \mathbf{b}_{\perp})$ are writing as an integral over $Q = |\mathbf{q}_{\perp}|$:

$$H_i(x, \mathbf{b}_{\perp}) = \int_0^\infty \frac{dQ}{2\pi} Q J_0(bQ) H_i^v(x, 0, Q^2), \tag{4.5}$$

where J_0 is the cylindrical Bessel function of order zero. After taking into account (3.6) in (4.4) and integrating out over Q, we find an explicit expression for the generalized parton distributions H_i in the IP space:

$$H_{1}(x,b) = -\frac{10k^{2}(x-1)^{3}e^{\frac{2b^{2}k^{2}}{\lg x}}}{\pi m^{2}(1+x)^{7}\lg x^{3}} \left(64b^{2}k^{4}(x-1) + \lg x(32k^{2}(x-1) + \left(16m^{2}(x-1) - 27k^{2}(x+1)\right)\lg x\right)\right),$$

$$H_{2}(x,b) = -\frac{480k^{2}(x-1)^{4}}{(1+x)^{7}\lg x}e^{\frac{2b^{2}k^{2}}{\lg x}},$$

$$H_{5}(x,b) = -\frac{30k^{2}(x-1)^{3}}{m^{2}(1+x)^{7}\lg x^{3}}e^{\frac{2b^{2}k^{2}}{\lg x}}\left(64b^{2}k^{4}(x-1) + 32k^{2}(x-1)\lg x - \left(8m^{2}(x-1) + 27k^{2}(1+x)\lg x^{2}\right)\right).$$

$$(4.6)$$

A plot of these GPDs can be performed numerically: It is seen from the plots in Fig.5 that the

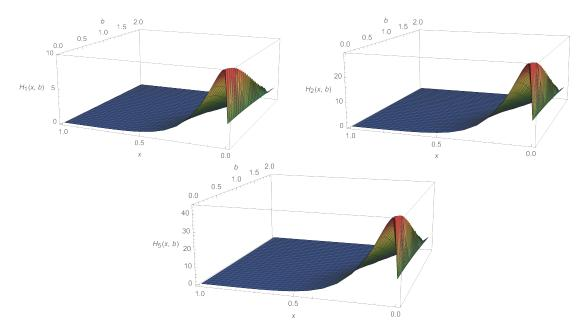


FIG. 5: Plot of $H_1(x,b)$, $H_2(x,b)$, $H_5(x,b)$ is generalized parton distributions in impact parameter space.

peak of the GPDs graphs in IP space decreases with increasing of the impact parameter b. In the thermal dilaton soft-wall model we only replace the dilaton parameter k with the temperature-dependent dilaton parameter K_T . This allows us to express the GPDs in the impact parameter space at finite temperature in the same way as in the zero temperature case. To do this, we replace k in the GPDs in (4.6) with K_T :

$$H_{1}(x,b,T) = -\frac{10K_{T}^{2}(x-1)^{3}e^{\frac{2b^{2}K_{T}^{2}}{\lg x}}}{\pi m^{2}(1+x)^{7}\lg x^{3}} (64b^{2}K_{T}^{4}(x-1) + \lg x(32K_{T}^{2}(x-1) + (16m^{2}(x-1) - 27K_{T}^{2}(x+1))\lg x)),$$

$$H_{2}(x,b,T) = -\frac{480K_{T}^{2}(x-1)^{4}}{(1+x)^{7}\lg x}e^{\frac{2b^{2}K_{T}^{2}}{\lg x}},$$

$$H_{5}(x,b,T) = -\frac{30K_{T}^{2}(x-1)^{3}}{m^{2}(1+x)^{7}\lg x^{3}})e^{\frac{2b^{2}K_{T}^{2}}{\lg x}} (64b^{2}K_{T}^{4}(x-1) + 32K_{T}^{2}(x-1)\lg x - (8m^{2}(x-1) + 27K_{T}^{2}(1+x)\lg x^{2}).$$

$$(4.7)$$

As is seen from Fig. 5 the plots of different H_i have similar behavior and peak at x = 0, despite different expressions in (4.7) for these GPDs. Comparing with the plots in Fig. 4, we observe that GPDs in IP space are more sensitive to temperature, as peaks of graphs in Fig. 5 decrease on temperature rising.

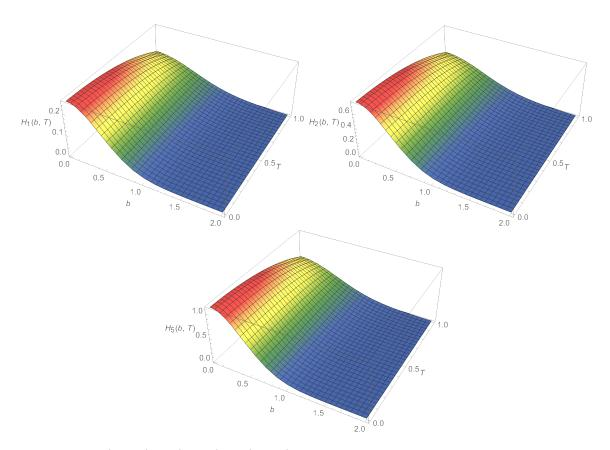


FIG. 6: Plot of $H_1(x, b, T)$, $H_2(x, b, T)$, $H_5(x, b, T)$ is generalized parton distributions in impact parameter space at finite temperature in x = 0.5.

V. DEUTERON TRANSVERSE CHARGE DENSITY

Transverse charge density ρ_{λ}^{+} in IP space is defined as a Fourier transform of the $\mathcal{T}_{\lambda\lambda}^{+}(Q^{2})$ form factors:

$$\rho_{\lambda}^{+}(\mathbf{b}_{\perp}) = \int \frac{d^{2}\mathbf{q}_{\perp}}{(2\pi)^{2}} e^{-i\mathbf{q}_{\perp} \cdot \mathbf{b}_{\perp}} \mathcal{T}_{\lambda\lambda}^{+}(Q^{2}). \tag{5.1}$$

It gives a probability that the charge is located at transverse separation b from the transverse center of momentum. The ρ_{λ}^{+} density of the spin-1 particle is related to the IP space 2-dimensional Fourier transform of the $Z_{1,2}$ GFFs [6]. In holographic QCD for the special $\tau = 6$ case one can obtain the following charge densities for deuteron [12]:

$$\rho_1^+(b) = \int_0^\infty \frac{dQ}{2\pi} Q J_0(bQ) Z_2(Q^2) ,$$

$$\rho_0^+(b) = \int_0^\infty \frac{dQ}{2\pi} Q J_0(bQ) Z_1(Q^2) .$$
(5.2)

Using holographic expressions (3.5) one can investigate transverse charge densities (5.2) numerically. In Fig. 7 a, we plot a 3-dimensional graph for the ρ_1^+ density, and in Fig.7 b we give its

2-dimensional projection in (b_x, b_y) plane. The shape of these plots coincides with 2-dimensional graphs plotted in [12].

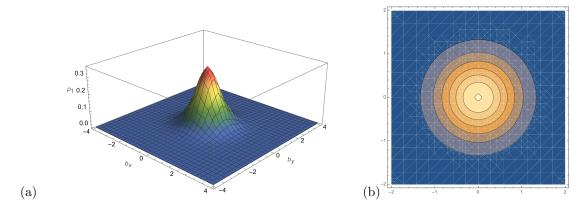


FIG. 7: Plot of $\rho_1^+(\vec{b}_\perp)$ transverse charge density of deuteron.

To have charge density in IP space we have to take into account in the (5.1) the finite-temperature $\mathcal{T}_{\lambda\lambda}^+(Q^2)$ in (2.24). This will lead to replacement in (5.2) the $Z_{1,2}(Q^2)$ form factors by the thermal ones $Z_{1,2}(Q^2,T)$:

$$\rho_1^+(b,T) = \int_0^\infty \frac{dQ}{2\pi} Q J_0(bQ) Z_2(Q^2,T) ,$$

$$\rho_0^+(b,T) = \int_0^\infty \frac{dQ}{2\pi} Q J_0(bQ) Z_1(Q^2,T) .$$
(5.3)

As is seen from the graphs in Fig. 8 the charge density peak is higher at the temperature T = 0 than at T = 1 fm⁻¹. This means the charge density peak decreases on temperature rising.

VI. SUMMARY

The found GFFs have the same shape as the ones obtained from EM FFs. The RMS radius obtained from GFFs is close to experimental data for the mass radius. The temperature dependence study of the radius becomes infinite starting from the critical value of the temperature. The shapes of plots of GPDs obtained from different form factors are the same. Such shape form is characteristic for the nucleons ([47]), pions ([49]) and vector mesons ([26]). The charge density peak in IP space is weakly sensitive to the temperature. This work's study can be extended to the non-zero skewness dependence of GPDs. The quantities describing the deuteron inner structure can also be studied, considering an interaction between nucleons. To this end, it is useful to extend the Argonne V18 potential, which includes spin and angular momentum interaction between nucleons, to five-dimensional space-time. This is the future perspective of the study.

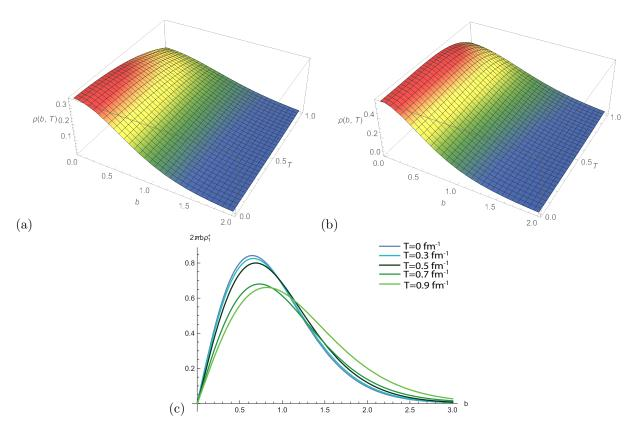


FIG. 8: Plot (a) is $\rho_1^+(b,T)$ charge density for Z_2 and (b) is $\rho_0^+(b,T)$ charge density for Z_1 of deuteron at finite temperature.

[1] J. M. Maldacena, Adv. Theor. Math. Phys. 2, 231 (1998), [arXiv:9711200 [hep-th]].

- [8] T. Gutsche, V. E. Lyubovitskij, I. Schmidt, A. Vega, Phys. Rev. D, 91, 11, 114001, (2015), [arxiv: 1501.02738 [hep-ph]].
- [9] N. Huseynova, Sh. Mamedov, J. Samadov, Chin. Phys. C 47, 013104, (2023), [arXiv:2204.06205 [hep-
- [10] E. Folco Capossoli, M. Martin Contreras, D. Li, A. Vega and H. Boschi-Filho, Chin. Phys. C 44, 064104, (2020), [arXiv:1903.06269 [hep-ph]].

^[2] S. S. Gubser, I. R. Klebanov and A. M. Polyakov, Phys. Lett. B 428, 105 (1998), [arXiv:9802109] [hep-th]].

^[3] E. Witten, Adv. Theor. Math. Phys. 2, 253 (1998), [arXiv: 9802150[hep-th]].

^[4] Z. Abidin, C. E. Carlson, Phys. Rev. D 77, 095007, (2008), [arXiv:0801.3839 [hep-ph]].

^[5] Z. Abidin and C.Carlson, Phys. Rev. D 79, 115003 (2009), [arXiv:0903.4818 [hep-ph]].

^[6] Z. Abidin, C. E. Carlson, Phys. Rev. D 78, 071502 (R), (2008), [arXiv:0808.3097 [hep-ph]].

^[7] T. Gutsche, V. E. Lyubovitskij, I. Schmidt, Phys. Rev. D 94, 11, 116006, (2016), [arXiv:1607.04124 [hep-ph]].

- [11] M. Rinaldi and V. Vento Phys. Rev. D **104**, 034016 (2021), [arXiv:2101.02616 [hep-ph]].
- [12] C. Mondal, D. Chakrabarti, X. Zhao, Eur. Phys. J. A 53, 106 (2017), [arXiv:1705.05808 [hep-ph]].
- [13] A. Karch, E. Katz, D. T. Son and M. A. Stephanov, Phys. Rev. D 74, 015005 (2006), [arxiv:0602229 [hep-ph]].
- [14] H. R. Grigoryan, A. V. Radyushkin, Phys. Rev. D **76**, 095007, (2007), [arXiv: 0706.1543 [hep-ph]].
- [15] Sh. Mamedov, B. B. Sirvanli, I. Atayev, N. Huseynova, Int. J. Theor. Phys., 56, 1861-1874, 6, (2017), [arXiv:1609.00167 [hep-th]].
- [16] N. Huseynova and Sh. Mamedov, Int. J. Theor. Phys. 54, 3799, (2015), [arxiv: 1408.5496 [hep-th]].
- [17] N. Huseynova, Sh. Mamedov, Int. J. Mod. Phys. A 34, 1950240, (2020), 35, [arXiv:1907.13477 [hep-ph]].
- [18] S. A. Mamedov and N. J. Huseynova, Int. Conf. on Modern Trends in Physics, 128-130, (2017).
- [19] Sh. Mamedov, Z. Hashimli, Sh. Jafarzade, Phys. Rev. D 108 (2023) 11, 114032, [arxiv: 2308.12392 [hep-ph]].
- [20] A. Vega and M. A. M. Contreras, Nucl. Phys. B 942, 410, (2019).
- [21] T. Gutsche, V. E. Lyubovitskij, I. Schmidt, A. Y. Trifonov, Phys. Rev. D, 99, 5, 054030, (2019), [arXiv:1902.01312[hep-ph]].
- [22] T. Gutsche, V. E. Lyubovitskij, I. Schmidt, and A. Y. Trifonov, Phys. Rev. D 99, 114023 (2019), [arXiv:1905.02577[hep-ph]].
- [23] T. Gutsche, V. E. Lyubovitskij, I. Schmidt, Nucl. Phys. B, 952, 114934, (2020), [arXiv:1906.08641[hep-ph]].
- [24] Sh. Mamedov, Sh. Taghiyeva, Eur. Phys. J. C, 81, 1080, (2021), [arXiv:2108.13513 [hep-ph]].
- [25] Sh. Mamedov, N. Nasibova, Phys. Rev. D, 104, 036010, (2021), [arXiv:2103.10494 [hep-ph]].
- [26] M. Allahverdiyeva, Sh. Mamedov, Eur. Phys. J. C 83, 5, 447, (2023), [arXiv:2302.03383 [hep-ph]].
- [27] Sh. Mamedov, N. Nasibova, Int. J. Mod. Phys. A 38, 24, (2023), 2350131, [arxiv: 2201.03324 [hep-ph]].
- [28] Sh. Mamedov, Sh. Taghiyeva, J. Korean Phys. Soc. 85, 541, (2024), [arxiv: 2208.07115 [hep-ph]].
- [29] Y. Dong and C. Liang, Int. J. Mod. Phys. Conf. Ser. 29 (2014), 1460229, [DOI:10.1142/S2010194514602294].
- [30] A. Airapetian et al.(HERMES), Nucl. Phys. B 842, 265 (2011), [arXiv:1008.3996 [hep-ex]].
- [31] M. Mazouz et al. (Jefferson Lab Hall A), Phys. Rev. Lett. **99**, 242501 (2007), [arXiv:0709.0450 [nucl-ex]].
- [32] W. Armstrong et al., (2017), [arXiv:1708.00888 [nucl-ex]].
- [33] A. Accardi et al., Eur. Phys. J. A52, 268 (2016), [arXiv:1212.1701 [nucl-ex]].
- [34] E. R. Berger, F. Cano, M. Diehl, and B. Pire, Phys. Rev. Lett. bf 87, 142302 (2001), [arXiv:hep-ph/0106192 [hep-ph]].
- [35] F. Cano and B. Pire, Eur. Phys. J. A19, 423 (2004), [arXiv:hep-ph/0307231 [hep-ph]].
- [36] W. Cosyn and B. Pire, Phys. Rev. D 98, 074020 (2018), [arXiv:1806.01177 [hep-ph]].

- [37] F. Cano and B. Pire, Proceedings, European Workshop, QCD-N'02, Ferrara, Italy, April 3-6, 2002, Nucl. Phys. A 711, 133 (2002), [arXiv:hep-ph/0206215 [hep-ph]].
- [38] A. Kirchner and D. Mueller, Eur. Phys. J. C32, 347 (2003), [arXiv:hep-ph/0302007 [hep-ph]].
- [39] I. V. Anikin, R. S. Pasechnik, B. Pire, and O. V. Teryaev, Eur. Phys. J. C 72, 2055 (2012), [arXiv:1112.1849 [hep-ph]].
- [40] M. Diehl, Generalized parton distributions, Phys. Rept. 388, 41-277 (2003), [arXiv:hep-ph/0307382].
- [41] C. Mondal, D. Chakrabarti, Eur. Phys. J. C 75, 261 (2015), [arXiv:1501.05489 [hep-ph]].
- [42] C. Mondal, J. Lan, K. Fu, S. Xu, Z. Hu, X. Zhao, J. P. Vary, SciPost Phys. Proc. 10, 036 (2022), [arXiv:2109.12921 [hep-ph]].
- [43] A. Vega, I. Schmidt, T. Gutsche, V. E. Lyubovitskij, Phys. Rev. D 83, 036001 (2011), [arXiv:1010.2815v3 [hep-ph]].
- [44] M. V. Polyakov, B. -D. Sun, Phys. Rev. D 100, 036003, (2019), [DOI:10.1103/PhysRevD.100.036003].
- [45] M. Burkardt, Int. J. Mod. Phys. A 18, 173-208 (2003), [arXiv: 0207047 [hep-ph]].
- [46] R. Wang, W. Kou, C. Han, J. Evslin, X. Chen, Phys. Rev. D 104, 074033, (2021), [arXiv:2108.03550 [hep-ph]].
- [47] A. Vega, I. Schmidt, T. Gutsche, V. E. Lyubovitskij, Phys. Rev. D 85, 096004, (2012), [arXiv:1202.4806 [hep-ph]].
- [48] P. E. Kolpakov, Basics of nuclear physics, (1968).
- [49] N. Kaur, N. Kumar, C. Mondal, H. Dahiya Nucl. Phys. B 934, 80-95, (2018), [arXiv:1807.01076 [hep-ph]].
- [50] C. Huang, B. Ma, Nucl. Phys. A 968, 14-22, (2017), [arXiv:1705.06399 [hep-ph]].
- [51] L. Bartolini, S. Bolognesi, S. B. Gudnason Phys. Rev. D 101, 086009, (2020), [arXiv:1912.01641 [hep-ph]].
- [52] Y. Kim, S. Lee, P. Yi JHEP **086**, 0904, (2009), [arXiv:0902.4048 [hep-ph]].
- [53] M. R. Pahlavani, J. Sadeghi, R. Morad, Phys. Rev. c 82, 025201, (2010), [arXiv:1309.06409 [hep-th]].
- [54] M. R. Pahlavani, R. Morad, Adv. High Energy Phys. A, 863268, (2014), [arXiv:1403.2501 [hep-th]].
- [55] D. Fujii, A. Iwanaka, M. Tanaka Phys. Rev. D 110, L091501, (2024), [arXiv:2407.21113 [hep-ph]]